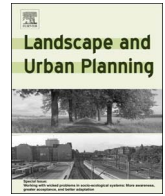




ELSEVIER

Contents lists available at ScienceDirect

Landscape and Urban Planning

journal homepage: www.elsevier.com/locate/landurbplan

Research Paper

Evaluation of satellite-derived building height extraction by CFD simulations: A case study of neighborhood-scale ventilation in Hong Kong

Weiwen Wang^{a,*}, Yong Xu^b, Edward Ng^{a,b,c}, Siegfried Raasch^d^a School of Architecture, The Chinese University of Hong Kong, Hong Kong Special Administrative Region, China^b Institute of Future Cities, The Chinese University of Hong Kong, Hong Kong Special Administrative Region, China^c Institute of Environment, Energy and Sustainability, The Chinese University of Hong Kong, Hong Kong Special Administrative Region, China^d Institute of Meteorology and Climatology, Leibniz Universität, Hannover, Germany

ARTICLE INFO

Keywords:

Building height extraction
Urban ventilation
Large-eddy simulation
High-density urban area

ABSTRACT

Computational fluid dynamics (CFD) techniques, such as large-eddy simulation (LES), are widely used in urban ventilation studies. Unfortunately, realistic building data required in CFD studies are not always available. In this study, LES of urban ventilation is used to assess building height extraction from different satellite images. As a case study, three sets of digital elevation data extracted from satellite images in an urban area of Mong Kok, Hong Kong, are assessed. Simulations of velocity ratio from the LES model are first validated by wind tunnel measurements, yielding a recommended local roughness length of 0.02 m. Wind characteristics in urban elevations extracted from two single satellite images and the fused result are then compared with those from realistic data in the same area, using identical LES settings. It is found that building height data retrieved from the WorldView-2 optical (stereo) images are of poor quality, as they underestimate higher buildings, which are deemed to be more important for pedestrian-level velocity ratios. The TerraSAR-X synthetic aperture radar (SAR) image and the fused results of SAR and stereo images are sufficient for CFD simulations of urban ventilation. This fusion provides a slight improvement over SAR images alone in reproducing urban geometric parameters, and it is superior in simulating more accurate wind profiles in the urban canopy.

1. Introduction

According to the World Health Organization, the urban population in 2014 accounted for 54% of the total global population, up from 34% in 1960, and it continues to grow. Rapid urbanization causes many problems such as urban heat islands and air pollution, which threaten the health of city inhabitants. Urban ventilation is one way of mitigating these problems (Arnfield, 2003; Shi, Zhu, Duan, Shao, & Wang, 2015; Wang, Zhou, Ng, & Xu, 2016; Wong, Nichol, & Ng, 2011). Good air ventilation is very important for high-quality and healthy living, particularly for high-density cities in tropical and subtropical regions with a hot and humid climate. Thermal comfort can be achieved by capturing natural wind. The neutral physiological equivalent temperature in summer in Hong Kong is around 28 °C. To achieve neutral thermal sensation in such conditions in a tropical and subtropical urban environment, a wind speed of 0.9–1.3 m/s is needed for a person wearing light clothing under shaded conditions (Ng & Cheng, 2012).

In the literature of urban air ventilation, various research methods have been used to describe the complex flows over urban environments. Computational fluid dynamics (CFD) techniques such as the Reynolds-

averaged Navier-Stokes (RANS) model, large-eddy simulation (LES), and direct numerical simulation (DNS) are among the commonly used tools (Britter & Hanna, 2003). Urban ventilation is strongly influenced by wind speed and direction, which in turn are affected by three-dimensional urban morphology (Ramponi, Blocken, de Coo, & Janssen, 2015; Skote, Sandberg, Westerberg, Claesson, & Johansson, 2005). Unfortunately, realistic digital elevations of urban areas required in CFD studies are not always available for open access, especially in the less-developed regions of the world where urban population growth is concentrated. Furthermore, surface geometries and urban morphologies are found to have a significant influence on urban heat islands (Unger, 2004), especially in regions with a hot and humid microclimate (Emmanuel & Johansson, 2006). High-resolution digital elevations have been extensively used in studies of urban climate and outdoor thermal comfort (Lindberg & Grimmond, 2010). Therefore, there is a need to develop methodologies for extracting building heights in urban areas from satellite images that can be used for, but not limited to, studies of urban ventilation.

Three kinds of building height extractions are available from remote sensing data: stereo photogrammetry technology with pairs of optical

* Corresponding author.

E-mail addresses: w.wang@cuhk.edu.hk (W. Wang), xuyong@cuhk.edu.hk (Y. Xu), edwardng@cuhk.edu.hk (E. Ng), raasch@muk.uni-hannover.de (S. Raasch).

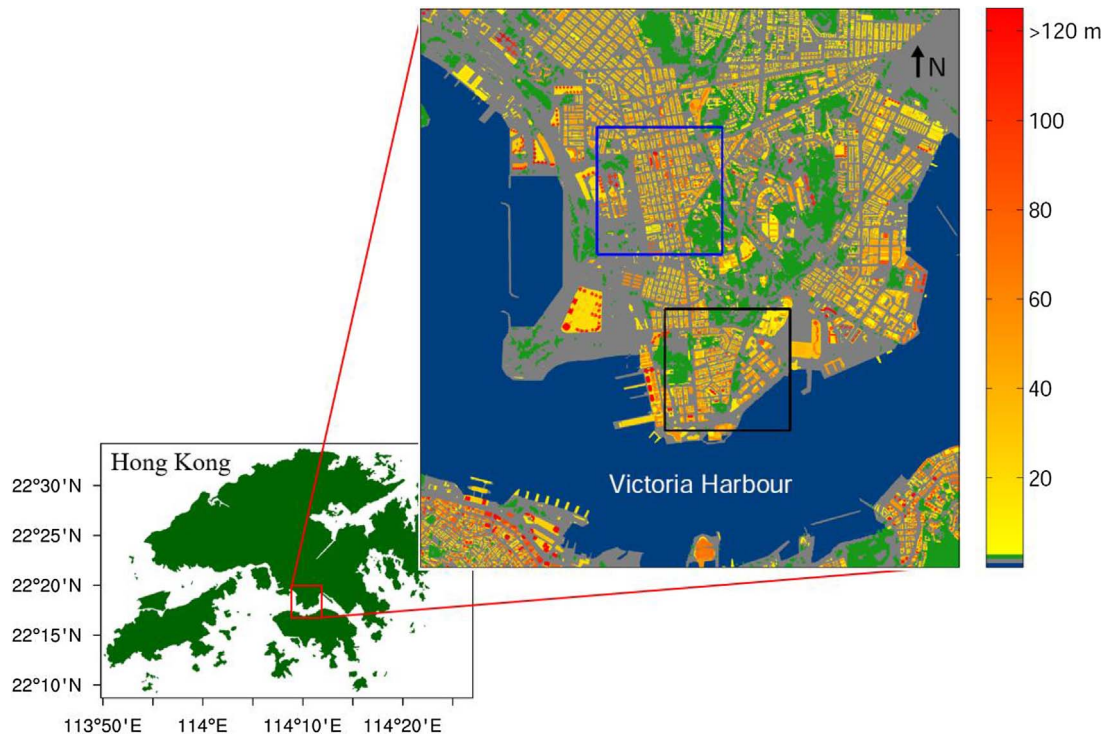


Fig. 1. A map of the study area. The small panel shows a shape map of Hong Kong. The Kowloon Peninsula is enlarged, and the colored map denotes land use types and building heights. The blue box encloses the $1.2 \text{ km} \times 1.2 \text{ km}$ neighbourhood used for building height extraction and evaluation at Mong Kok, while the black box encloses the $1.2 \text{ km} \times 1.2 \text{ km}$ neighbourhood of the wind tunnel site at Tsim Sha Tsui. (For interpretation of the references to colour in this figure legend, the reader is referred to the web version of this article.)

images (hereafter referred to as stereo images), synthetic aperture radar (SAR) technology, and light detection and ranging (LiDAR) technology. However, there are limitations to these methods: (1) stereo images tend to underestimate the height of tall buildings, and taller buildings produce larger errors (Eckert & Hollands, 2010); (2) the interferometry of SAR provides noisy and incomplete data, particularly for high-density urban areas where the mutual interference of surrounding buildings is significant (Colin-Koeniguer & Trouve, 2014); and (3) LiDAR data are expensive and limited by flight restrictions for applications in large urban areas (Zhou & Zhou, 2014). Therefore, recent studies have also been devoted to the integrated use of different kinds of data for building height retrieval (Sportouche, Tupin, & Denise, 2011).

The objective of the present study is to assess the performance of building height extractions from different kinds of satellite images for potential use in urban ventilation studies with CFD techniques. As a case study, we perform CFD simulations and assessment in high-density urban areas on the Kowloon Peninsula, Hong Kong. A map of the study area is shown in Fig. 1. The high-density urban areas on the Kowloon Peninsula are enlarged from a shape map of Hong Kong. In the enlarged Kowloon Peninsula map, the blue box encloses the $1.2 \text{ km} \times 1.2 \text{ km}$ neighbourhood used for building height extraction and evaluation at Mong Kok. The black box encloses the $1.2 \text{ km} \times 1.2 \text{ km}$ neighbourhood of the wind tunnel site at Tsim Sha Tsui, which is used for validating the CFD codes in this study.

Evaluation of building height extraction from satellite images from the perspective of an application, that is, urban ventilation, has rarely been attempted to date as far as we know. What affects pedestrian comfort directly is the wind flow within cities, and the local turbulence level in particular (Britten & Hanna, 2003). We therefore use an LES model to produce CFD simulations in this study. LES overcomes the deficiencies of RANS by explicitly resolving large, energy-containing turbulent eddies and parameterizing only small (subgrid)-scale turbulence (Rodi, Ferziger, Breuer, & Pourquie, 1997; Tamura, 2008). The dimensionality, spatial resolution, and turbulence intensity that an LES model can handle are superior to those of most other methodologies,

and sometimes also to those of other CFD models, such as RANS and DNS (Castillo, Inagaki, & Kanda, 2011). LES provides not only mean flow fields but also instantaneous turbulences, which are especially important for human comfort at the pedestrian level in the urban canopy layer (Keck, Raasch, Letzel, & Ng, 2014).

2. Data and methodology

2.1. Wind tunnel measurements

In air ventilation assessment (AVA) studies, we are especially interested in pedestrian-level wind velocity. The wind velocity ratio (VR) is used as an indicator, which is calculated by $VR = V_p/V_\infty$, where V_p is the wind velocity at the pedestrian level (2 m above the ground), and V_∞ is the wind velocity at the top of the wind boundary layer and is not affected by ground roughness. Velocity ratios measured from a wind tunnel model are used to compare with LES results in this study and are taken from the “Urban Climatic Map and Standards for Wind Environment – Feasibility Study” (Hong Kong Planning Department, 2008). The wind tunnel model tests were undertaken in accordance with the international practice requirements stipulated in the *Australasian Wind Engineering Society Quality Assurance Manual* (AWES-QAM-1-2001) and the *American Society of Civil Engineers Manual and Report on Engineering Practice for Wind Tunnel Studies of Building and Structures* (No. 67). The scale of the model was 1:400. Wind velocities were measured at 5 mm from the ground, which corresponds to 2 m. The top of the boundary layer was 500 m. The wind tunnel site at Tsim Sha Tsui, Kowloon, was chosen for comparison. Locations of all 94 test points at this site are shown in Fig. 2. Green dots denote test point group A (TSA, 31 points), blue dots denote test point group B (TSB, 29 points), and red dots denote test point group C (TSC, 34 points).

2.2. Neighborhood-scale urban elevations

In the present study, actual (measured) urban elevations (buildings)

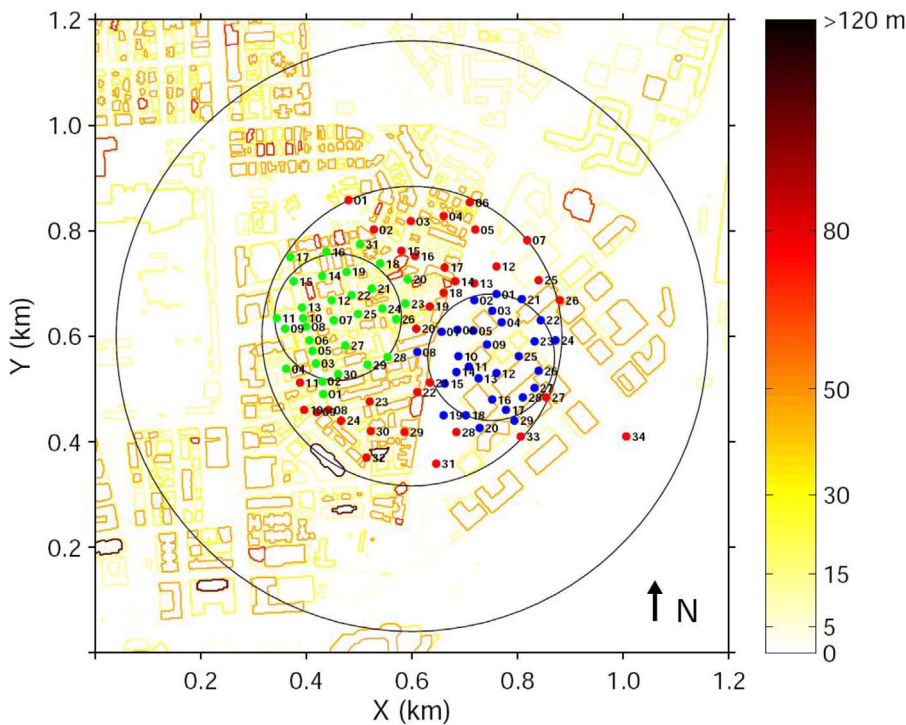


Fig. 2. Locations of test points at the wind tunnel site Tsim Sha Tsui for comparison with results from PALM. Green dots denote test point group A (TSA), blue dots denote test point group B (TSB), and red dots denote test point group C (TSC). The largest circle is used to define this site in the wind tunnel test, and the middle and two small circles are used as a location reference for the grouped test points. The colored bar describes building heights on the site. (For interpretation of the references to colour in this figure legend, the reader is referred to the web version of this article.)

in two neighborhoods on the Kowloon Peninsula provided by the Hong Kong Planning Department are utilized as topography input for the LES model. One is the same as the wind tunnel site Tsim Sha Tsui, shown in Fig. 2. The other is the same area used in Xu, Ma, Ng, and Lin (2015) which jointly uses high-resolution WorldView-2 stereo images and multi-temporal TerraSAR-X SAR images to retrieve building heights in this high-density urban area of Mong Kok (Fig. 3a). Both are 1.2 km × 1.2 km and have a horizontal resolution of 2 m. The satellite-derived methodology for retrieving building heights in urban areas using both stereo and SAR images assumes that the building footprints are known and involves two main stages: first, estimated initial building heights are retrieved from stereo and SAR images, respectively; second, according to an object-based fusion approach, the initial building heights are then combined. The bias of building heights between actual data and data extracted from stereo images, SAR images, and the fused result of the two kinds of images is given in Fig. 3b–d, respectively.

A boxplot is attached to Fig. 3, and to other contour maps in this study, to describe statistics of the contoured parameter. In each box of the boxplot, the central mark is the median, the edges of the box are the 25th and 75th percentiles, and the whiskers extend to the most extreme data points (McGill, Tukey, & Larsen, 1978). The outlier algorithm of boxplots, which is not necessary for our purpose here, is ignored.

2.3. LES model and experiments

The LES model used in this study is the Parallelized LES Model (PALM), which has been used since 1997 (Raasch & Schröter, 2001). This LES model has been validated for simulating flows and turbulence characteristics at the street-canyon and neighbourhood scale (Letzel, Krane, & Raasch, 2008) and has been widely used in studies of urban street-canyon flows in recent years (Inagaki, Castillo, Yamashita, Kanda, & Takimoto, 2011; Kanda, Inagaki, Miyamoto, Gryschka, & Raasch, 2013; Park & Baik, 2014; Park, Baik, Raasch, & Letzel, 2012; Razak, Hagishima, Ikegaya, & Tanimoto, 2013; Wang, Ng, Yuan, & Raasch, 2017). The code used in this study is PALM version 4.0 (Maronga et al., 2015).

As we are focusing mainly on VR, the input wind speed is not very important, and if high wind speed is used, more computational time

will be needed because the time step must be shorter. Therefore, a wind speed of 1.5 m/s is prescribed to save computational time. The time step sizes are optimized in PALM. Horizontal grid sizes are equidistantly 2 m. The vertical grid spacing is 2 m below 300 m and stretched with a stretch factor of 1.08 above. CFD equations are spatially discretized on an Arakawa-C grid. Scalar variables are defined at the grid centers, while velocity components are shifted by half of the grid spacing. Therefore, horizontal wind velocity output from the 1 m and 3 m levels is linearly interpolated (averaged) to obtain V_p at 2 m above the ground. V_∞ is derived from 500 m to be comparable with wind tunnel tests. The total simulation time is 6 h. The first 4 h are excluded in the analysis of the results, as the turbulences need this time to spin-up. The simulated results from the 5th to the 6th hours are averaged for analysis. For the comparison with wind tunnel measurements, east (90°) wind input is simulated. East and southwest (225°) winds, the prevailing annual and summer winds in Hong Kong, respectively, are simulated for assessment of building height extraction from satellite images. The no-slip bottom boundary condition with a Prandtl layer and the free-slip top boundary condition are applied to horizontal velocity components. As the targeted area is surrounded by urban areas, a simple cyclic (periodic) boundary condition setup in both the streamwise and spanwise directions is sufficient for the task. The simulations are restricted to neutral atmospheric stratification; that is, thermal effects are not considered.

3. Zonal comparison with wind tunnel tests

The best available verification of LES results at present is a cross-comparison of results computed by LES with those derived from wind tunnel measurements. Meanwhile, a zonal comparison is more representative and meaningful than a point-to-point direct comparison (Schatzmann & Leitel, 2011). In this comparative analysis, the test points are classified into a few groups in terms of their street types and ground coverage (Table 1). For street types, 94 test points are divided into 4 groups: main streets, narrow streets with parallel flow, narrow streets with canyon flow (streets perpendicular to the input wind direction), and waterfront/open spaces. For ground coverage, all test points are divided into 3 groups: low ground coverage refers to grids with

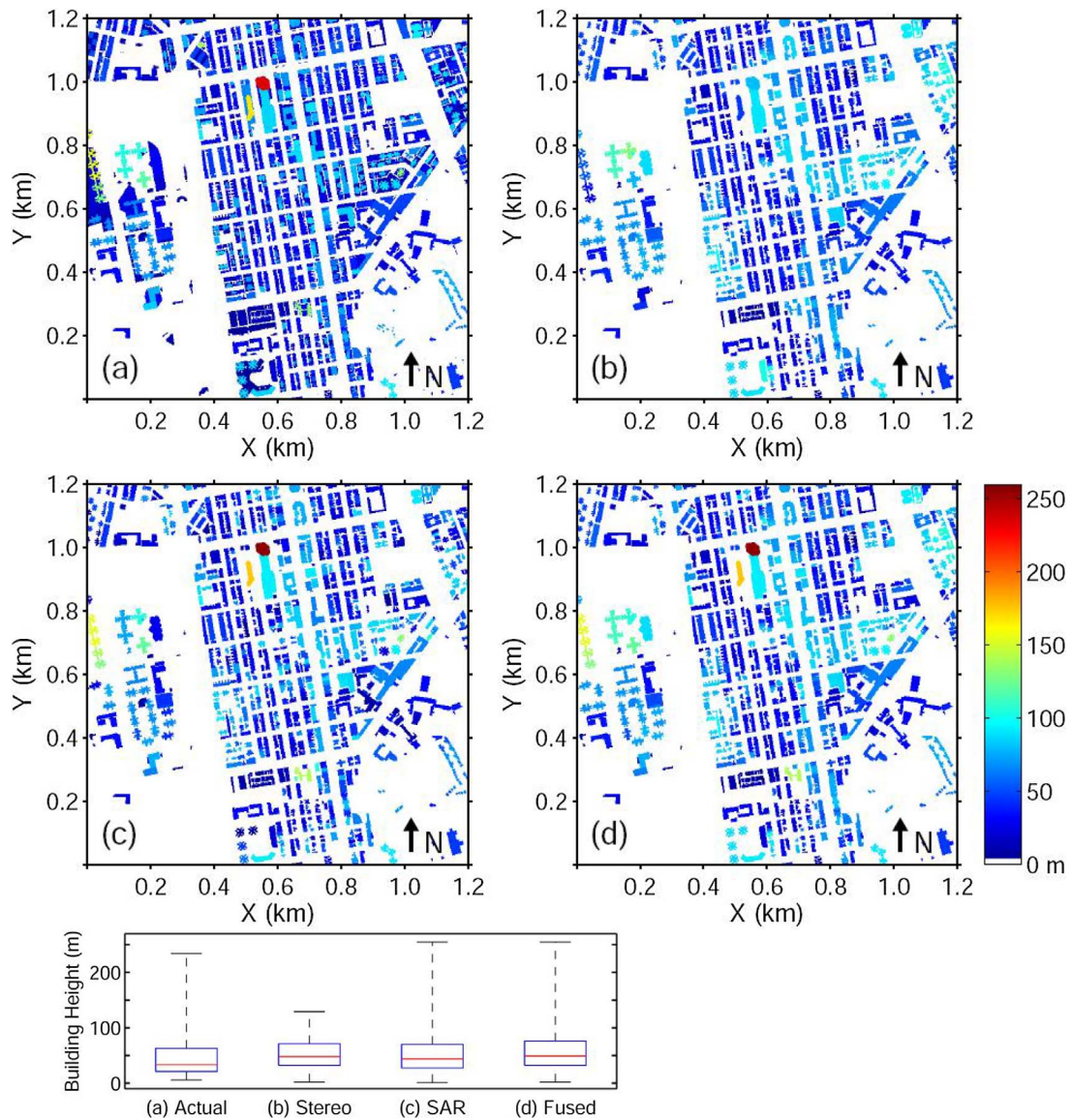


Fig. 3. (a) Actual urban elevations (buildings) in a 1.2 km × 1.2 km neighborhood in Mong Kok. Bias between actual data and data extracted from (b) stereo images, (c) SAR images, and (d) fused result of the two kinds of images. The boxplot describes statistics of building heights in 4 sets of data. Refer to the text for more details regarding boxplot statistics.

coverage not greater than 20%, high ground coverage refers to grids with coverage greater than 50%, and mid ground coverage refers to those in between. Ground coverage is calculated in a 100 m × 100 m grid where the test point is centered. This simple two-dimensional

ground coverage ratio, which is readily available, can be used to predict the area’s mean pedestrian-level ventilation (Ng, Yuan, Chen, Ren, & Fung, 2011). Finally, the mean of all test points in the entire assessment area is considered as one last sample (Table 1).

Table 1

A zonal comparison of velocity ratio (VR) between large-eddy simulation (LES) and wind tunnel (WT) results. The roughness length is 0.02 m for the LES results in the last column.

Zones of urban morphology	Test points	VR (WT)	VR (LES)	
Zone by street types	Main streets	TSB02, TSB06–07, TSB10, TSB14–15, TSB19, TSC05, TSC13–14, TSC21, TSC28, TSC31	0.24	0.28
	Narrow streets (parallel flow)	TSA07–09, TSA14–15, TSA18–19, TSA23–25, TSA28–30, TSB08, TSB23–24, TSC02, TSC06, TSC11, TSC15–18, TSC22–23, TSC29–30	0.22	0.22
	Narrow streets (canyon flow)	TSA01–06, TSA10–13, TSA16–17, TSA20–22, TSA26–27, TSA31, TSB01, TSB03–05, TSB09, TSB11–13, TSB16–18, TSB20–22, TSB25–29, TSC01, TSC03–04, TSC07–10, TSC12, TSC19–20, TSC24–27, TSC32–33	0.15	0.12
Zone by ground coverage (GC)	Waterfront/open spaces	TSC34	0.33	0.32
	Low GC (< = 20%)	TSA17, TSB10–11, TSB14, TSB23–25, TSC23, TSC34	0.23	0.20
	Mid GC (> 20% & < = 50%)	TSA01–02, TSA12, TSA14–16, TSA25, TSA28–30, TSB04–09, TSB12–13, TSB15, TSB22, TSB26–29, TSC03, TSC08–11, TSC21–22, TSC24, TSC27, TSC29–31, TSC33	0.21	0.18
	High GC (> 50%)	TSA03–11, TSA13, TSA18–24, TSA26–27, TSA31, TSB01–03, TSB16–21, TSC01–02, TSC04–07, TSC12–20, TSC25–26, TSC28, TSC32	0.15	0.17
Entire assessment area	Mean of all 94 test points	0.18	0.17	

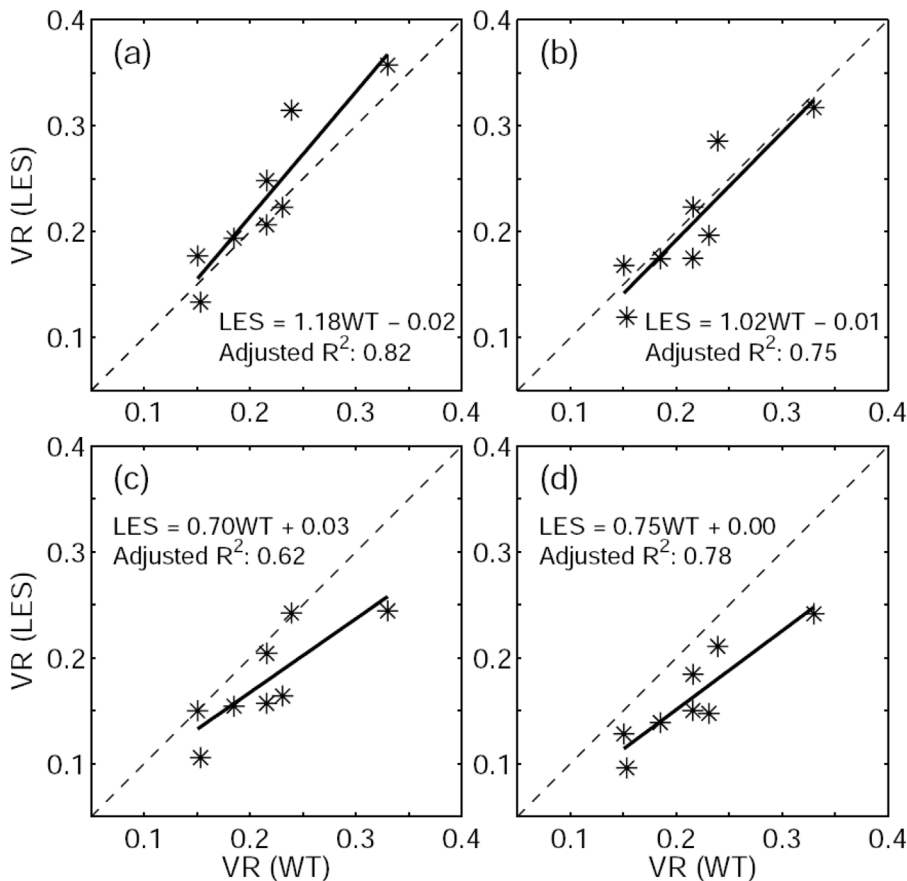


Fig. 4. Scatter plots (stars) and linear regressions (solid lines) of zonal averaged velocity ratio (VR) from wind tunnel (WT) measurements and large-eddy simulation (LES) results, with a roughness length of (a) 0.01 m, (b) 0.02 m, (c) 0.05 m, and (d) 0.1 m given in the LES model. The regressed linear models and adjusted r-squares (R^2) are given in the plots.

Pedestrian-level ventilation, or VR, which serves as an indicator for urban planners to assess the effect of developments and redevelopments, is highly influenced by complex urban geometry. VR is therefore highly site-dependent, but sensitivity tests are required to quantify the influence of numerical parameters. LES settings described in the previous section, such as grid spacing, boundary conditions, input wind speed, and spin-up and averaging time, are prescribed from a number of PALM experiments and previous studies (Kanda et al., 2013; Keck et al., 2014; Letzel et al., 2012). Apart from these setups, we found that the local roughness length in PALM is an important parameter that influences the overall VRs significantly. Fig. 4 compares a set of simulations using different roughness lengths and their linear regressions with wind tunnel results. Zoned VRs calculated in LES with a roughness length of 0.02 m are found to be most comparable with those measured from the wind tunnel test (Fig. 4b). Zoned VR values from both the wind tunnel and LES are listed in the last two columns of Table 1. While larger roughness lengths are utilized in LES—for example, 0.05 m and 0.1 m, as shown in Figs. 4c and d, respectively—zoned VRs are underestimated compared with those from wind tunnel measurements. In contrast, a smaller roughness length adopted in PALM results in overestimation of zoned VRs compared with the wind tunnel (Fig. 4a).

Fig. 5 compares the spatial differences of VRs calculated by LES between roughness lengths of 0.02 m and 0.1 m. Higher (lower) VRs are denoted by a cooler (warmer) color. Previous wind tunnel and CFD studies in Hong Kong have indicated a VR of about 0.3 near waterfront and open spaces, and 0.05–0.1 in streets and congested urban spaces (Ng, 2009). Fig. 5a suggests that an overall VR computed by LES with a roughness length of 0.02 m is in line with previous experimental and computational studies. While a roughness length of 0.1 m results in a systematic reduction in the overall VR, it is still within a reasonable range (Fig. 5b). In general, the differences are larger in regions with a higher absolute VR, about 0.04–0.08 lower in Fig. 5b than in a. Large

differences are found only in a few localized areas. For validation of building height extraction in the next section, we conduct LES runs with roughness lengths of both 0.02 m and 0.1 m. The choice of 0.1 m is in view of the local roughness length possibly being underestimated in the wind tunnel model, as complex objects in the city, such as traffic, advertisement boards, and air conditioners along building walls, are not included. Taking these into consideration, a roughness length of 0.1 m is the default setting in PALM and has been commonly adopted in previous studies (Letzel et al., 2008; Park et al., 2012).

4. Evaluation of building height extraction

A total of 16 LES experiments, including four types of urban topography data (actual, stereo, SAR, and fused), two roughness lengths (0.02 m and 0.1 m), and two input wind directions (east and southwest), are conducted to carry out this analysis. The performance of building height extraction for AVA purposes is defined by the difference in LES-calculated VR between extracted and actual topography. The smaller the bias is, the better the performance. As the simulated VR is highly site-dependent and is sensitive to many aspects, we describe the assessment process in terms of the effects of average size (grid sensitivity test for calculating site-averaged VR), wind direction and roughness length, building height, and the ways in which the fused satellite images are better than extraction from a single type of satellite image.

4.1. Effects of average size

Horizontal distributions of LES-computed VR with wind input from the east (southwest) with actual topography and satellite-extracted topography are given in Fig. 6 (Fig. 7). Urban planners and researchers care about the site-averaged VR. We select two kinds of grid sizes to

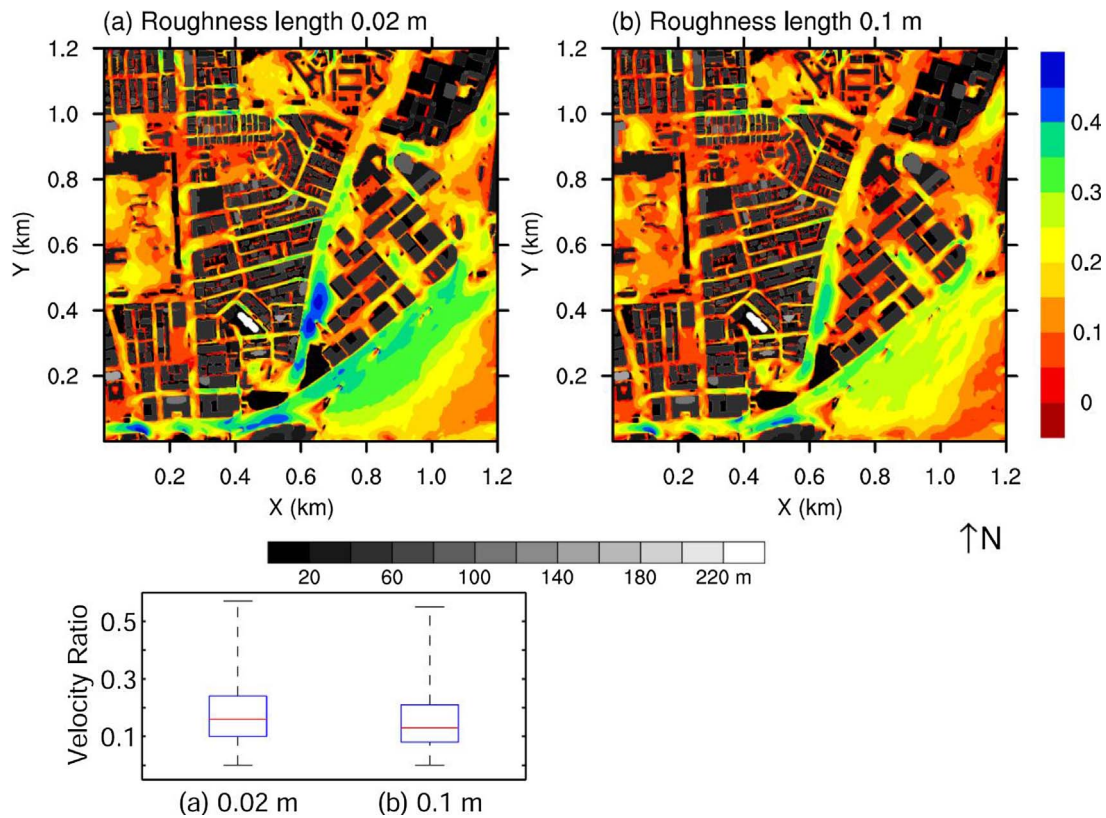


Fig. 5. LES-computed VR at the wind tunnel site Tsim Sha Tsui, Kowloon. The roughness length is (a) 0.02 m, and (b) 0.1 m. The vertical (horizontal) colored bar describes VR (building height). The boxplot describes statistics of VR in both LES experiments.

check whether the comparative results are sensitive to this average size. One is $100\text{ m} \times 100\text{ m}$ while the other is $50\text{ m} \times 50\text{ m}$, with a unique buffer width of 250 m. A buffer width of 250 m fulfills the requirement of AVA (Ng, 2009), as the tallest building in the research area is 255 m (Fig. 3). Generally, it is suggested that simulated results in the outer regions near the horizontal boundary are not reliable. The assessment areas are enclosed in dashed boxes in Figs. 6 and 7.

Table 2 lists all the root mean square errors (RMSEs) of LES-calculated VRs between satellite-extracted and actual topography. The largest and smallest values in each row are highlighted, bolded for the largest value and underlined for the smallest value. Referring to the average size, the results can be classified into 4 groups: first, roughness length 0.02 m and east wind (rows 1 and 2); second, roughness length 0.02 m and southwest wind (rows 3 and 4); third, roughness length 0.1 m and east wind (rows 5 and 6); and fourth, roughness length 0.1 m and southwest wind (rows 7 and 8). It is found that the average sizes do not change the order of RMSEs from three sets of topography in the first and fourth groups. In the second group, an average size of $100\text{ m} \times 100\text{ m}$ homogenizes the difference in the zonally averaged VR in three sets of topography (row 3), homogenization that cannot be seen from an average size of $50\text{ m} \times 50\text{ m}$ (row 4). The average size has a slight effect on the RMSE order of the third group, as can be seen from rows 5 and 6 of Table 2. We presume that the effects of average size, $50\text{ m} \times 50\text{ m}$ or $100\text{ m} \times 100\text{ m}$, on the overall RMSEs are not significant, as these two average sizes do not practically change the order of RMSEs from the three sets of topography. The scatter plots and linear regressions in Figs. 8 and 9 are produced with samples from an average size of $50\text{ m} \times 50\text{ m}$, which obtains more samples than an average size of $100\text{ m} \times 100\text{ m}$. Figs. 8 and 9 will be interpreted in the next section in association with the effects of wind direction and roughness length.

4.2. Effects of wind direction and roughness length

RMSEs in Table 2 suggest that building height data extracted from stereo images are of poor quality compared with the other two methods. A comparison of SAR and the fused results shows that the fused results perform better when given a roughness length of 0.1 m and southwest wind (rows 7 and 8), while the SAR result is slightly better in other cases. Figs. 8 and 9 further demonstrate the performance of data retrieved from different methods. The stereo result has a large bias from the actual topography in the LES experiment with east wind (Fig. 8a and d), while it performs better in the LES experiment with southwest wind (Fig. 9a and d). The performances of SAR and the fused results are close to each other and reasonable in the LES experiment with east wind (Fig. 8b, c, e, and f). In the LES experiment with southwest wind, a roughness length of 0.02 m results in a slight overestimation of the large VRs with both SAR and fused images (Fig. 9b and c, regressed lines), but a roughness length of 0.1 m may fix this overestimation (Fig. 9e and f). According to Table 2 and Figs. 8 and 9, we can preliminarily deduce that SAR images and the fused images are suitable for numerical simulations of urban ventilation, while stereo images alone may be not good enough.

The overall VR is larger with easterly input than with southwesterly input (Figs. 6 and 7). Street orientations in the area could be the main contributor. This is supported by comparing the frontal area index (FAI), which is defined as the frontal area of buildings in a certain wind direction over a site area (Xu et al., 2017). Fig. 10 demonstrates FAIs calculated from site areas of $100\text{ m} \times 100\text{ m}$, with east wind cases in the upper panels and southwest wind cases in the lower panels. The maximum FAI in the upper panels is about 1.2, while the maximum FAI in the lower panels reaches 2.0. This is deemed to be the major reason why the overall VR is larger with east wind than with southwest wind input.

The roughness lengths for Figs. 6 and 7 are both 0.02 m. The

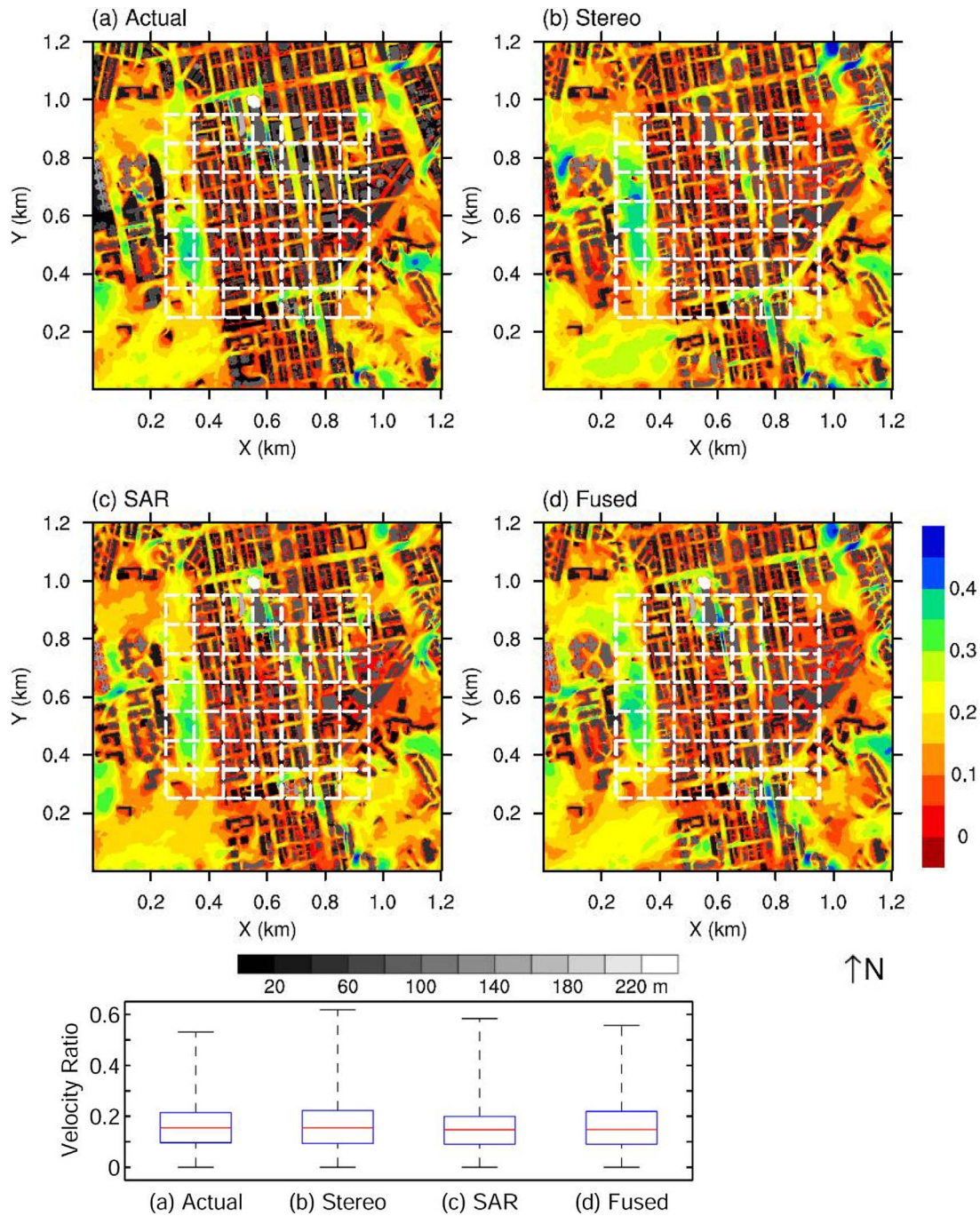


Fig. 6. LES-computed VR in (a) actual topography, (b) topography retrieved from stereo images, (c) topography retrieved from SAR images, and (d) fused results of the two images. The dashed boxes enclose the assessment area and denote the 100 m × 100 m domains for the zonal average. The vertical (horizontal) colored bar describes VR (building height). The roughness length is 0.02 m. Wind input is from the east. The boxplot describes statistics of VR in the four simulations.

horizontal distributions of VR for 0.1 m roughness length are not shown. The spatial patterns are like those in Figs. 6 and 7, but with systematically lower VR values, which can be referred to the boxplot in Fig. 5. Alternatively, we evaluate the impact of roughness length on ventilation by comparing the probability of VR taken from random test points inside the assessment area (Fig. 11). In this analytical procedure, all street grid points in each LES experiment are stored in a one-dimensional array, and 10,000 test points are randomly taken from each array to calculate the probability. The random function calculates the interval between test points using a normal distribution with a mean of the array size divided by the number of test points (10,000) and a standard deviation of 25% of the mean; thus, the test points are

randomly spread throughout the entire assessment area. Furthermore, sensitivity tests were conducted regarding the number of test points, and no significant differences were found when the number of test points was larger than 10,000, which means that 10,000 test points are sufficient to produce the probability graphs in Fig. 11.

Generally, 0.02 m roughness length increases the probability of higher VR and decreases the probability of lower VR compared to 0.1 m roughness length (Fig. 11). But the value dividing higher and lower VR is rather case-dependent. In the simulations of actual building data, for example, 0.02 m roughness length increases (decreases) the probability of VR above (below) around 0.15 with east wind input (Fig. 11a), while in the southwest wind experiment, the dashed and solid lines cross at

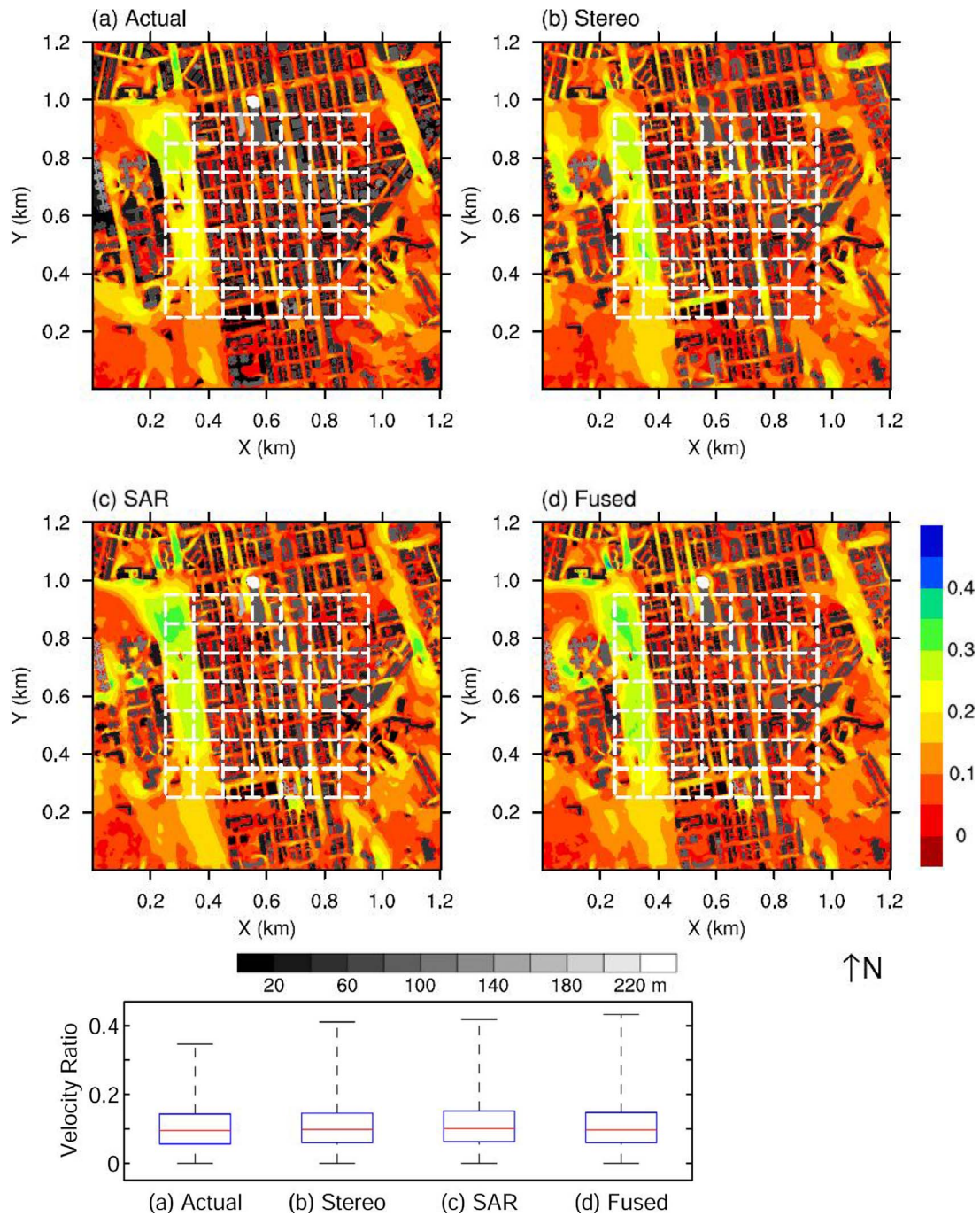


Fig. 7. LES-computed VR in (a) actual topography, (b) topography retrieved from stereo images, (c) topography retrieved from SAR images, and (d) fused results of the two images. The dashed boxes enclose the assessment area and denote the 100 m × 100 m domains for the zonal average. The vertical (horizontal) colored bar describes VR (building height). The roughness length is 0.02 m. Wind input is from the southwest. The boxplot describes statistics of VR in the four simulations.

Table 2
Root mean square errors (RMSEs) of VR between satellite-extracted and actual building heights in different LES experiments (roughness lengths and wind directions) and average sizes. The largest (smallest) value in each row is bolded (underlined).

Row No.	Roughness length (m)	Wind direction	Average size	RMSEs Stereo	RMSEs SAR	RMSEs Fused
1	0.02	East	100 m × 100 m	0.046	0.023	0.029
2	0.02	East	50 m × 50 m	0.053	0.032	0.035
3	0.02	Southwest	100 m × 100 m	0.023	0.023	0.023
4	0.02	Southwest	50 m × 50 m	0.032	0.027	0.029
5	0.1	East	100 m × 100 m	0.040	0.026	0.028
6	0.1	East	50 m × 50 m	0.046	0.035	0.035
7	0.1	Southwest	100 m × 100 m	0.017	0.014	0.009
8	0.1	Southwest	50 m × 50 m	0.023	0.020	0.016

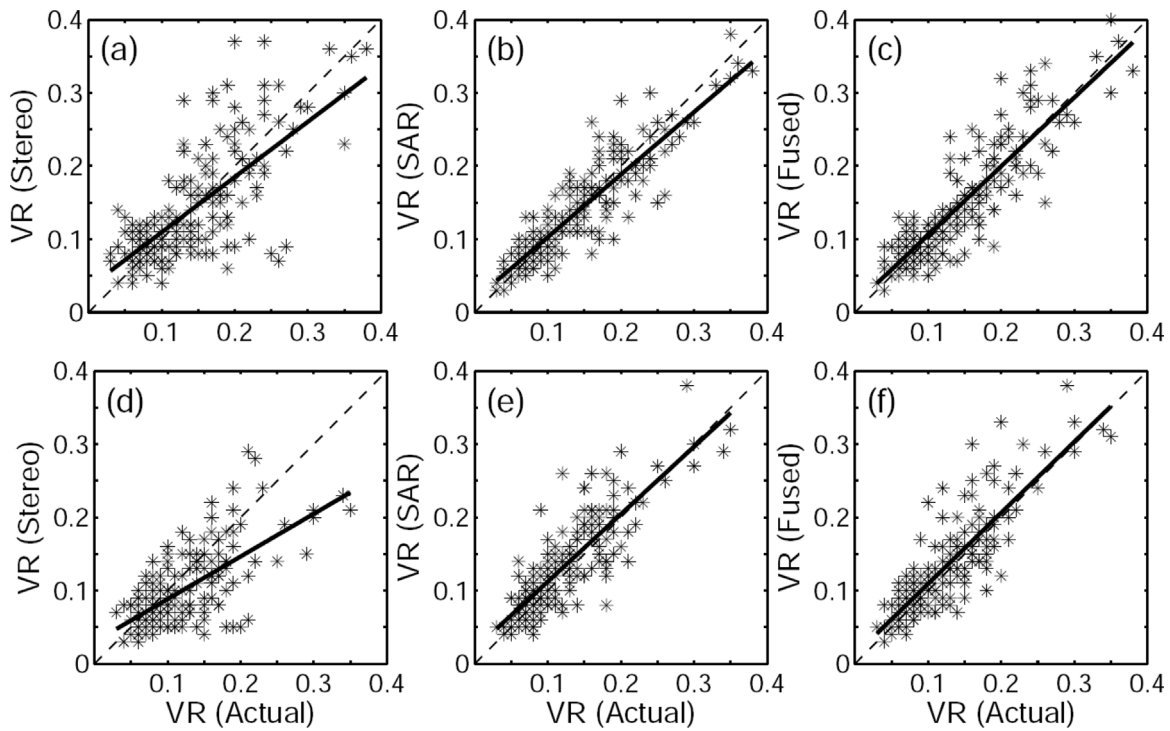


Fig. 8. Scatter plots (stars) and linear regressions (solid lines) of LES-computed VR with actual topography and topography extracted from (a, d) stereo images, (b, e) SAR images, and (c, f) fused results of the two images. The roughness length is 0.02 m (0.1 m) for a–c (d–f). Average size is 50 m × 50 m. Wind input is from the east.

about 0.2–0.3, and the difference in VR below 0.15 is very small (Fig. 11e). Similar situations are found in other cases in Fig. 11. Effects of roughness length are significant but rather complicated.

The effects of the roughness length setting are complicated and highly associated with building shapes and input wind direction. Change in the input wind direction causes modifications in local (subdomains in the neighborhood) urban morphology and geometry

parameters in AVA, such as the frontal area density. The local roughness length takes effect when the wind sweeps across the ground and walls. The higher the proportion of ground and walls the wind sweeps across, the larger the friction effects on the wind. Therefore, wind direction and roughness length affect air ventilation in combination, both locally and globally.

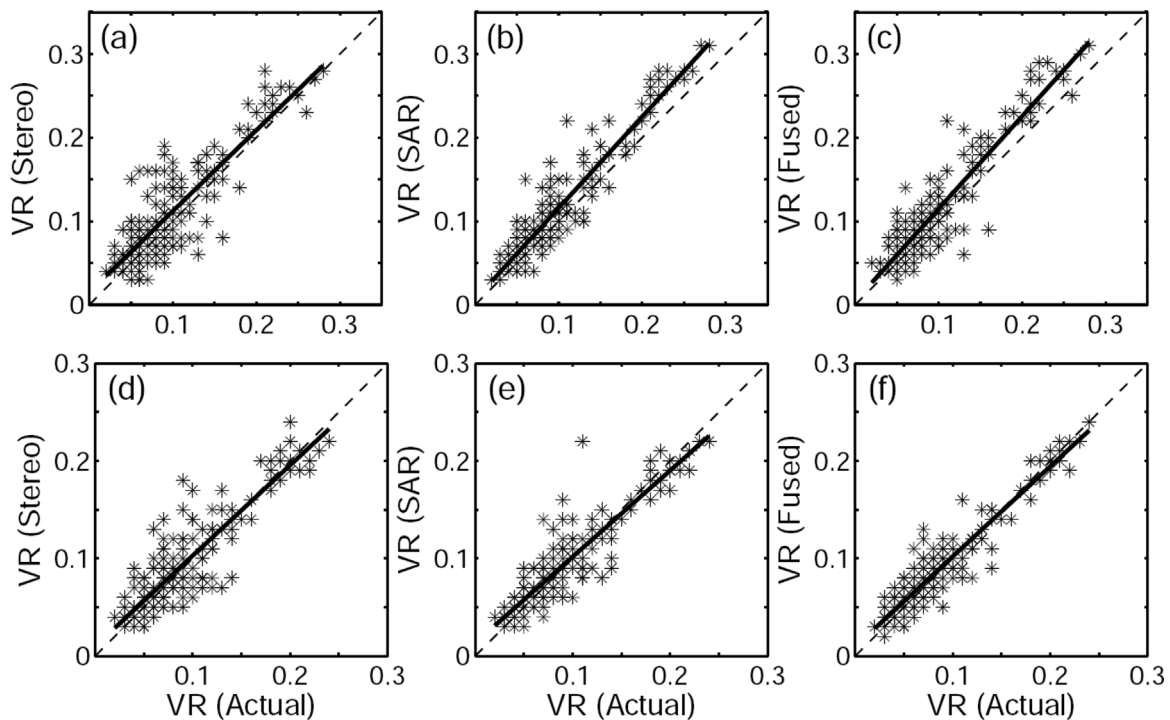


Fig. 9. Scatter plots (stars) and linear regressions (solid lines) of LES-computed VR with actual topography and topography extracted from (a, d) stereo images, (b, e) SAR images, and (c, f) fused results of the two images. The roughness length is 0.02 m (0.1 m) for a–c (d–f). Average size is 50 m × 50 m. Wind input is from the southwest.

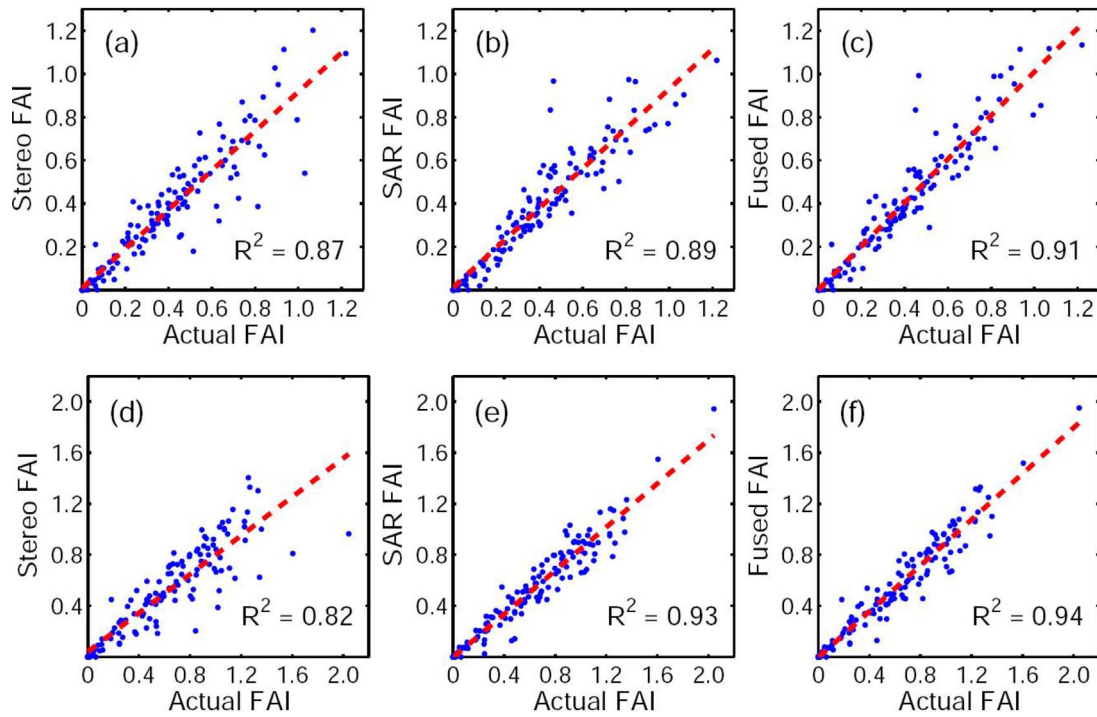


Fig. 10. Scatter plots (dots) and linear regression (dashed lines) of frontal area index (FAI) calculated from actual building data and building data retrieved from stereo images (a, d), SAR images (b, e), and fused results (c, f). The upper panels (a–c) are east wind input and the lower panels (d–f) are southwest wind input.

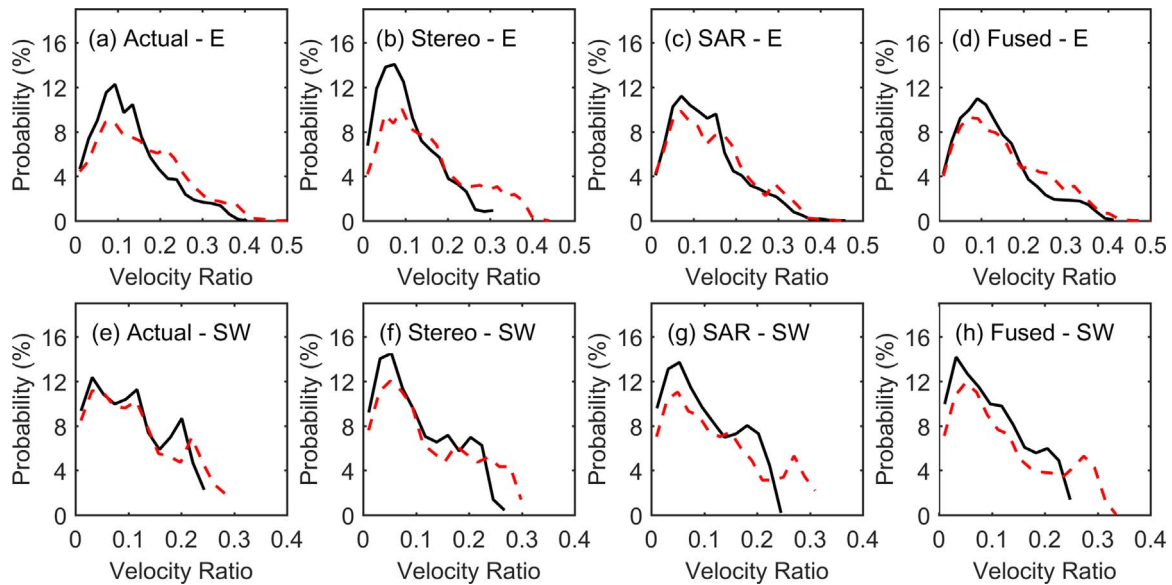


Fig. 11. The probability of VRs taken from random test points in the assessment area of 16 LES experiments. Upper panels are east (E) wind input and lower panels are southwest (SW) wind input. Dashed (solid) lines represent a roughness length of 0.02 m (0.1 m).

4.3. Effects of building height

Using the average absolute difference from measured data to evaluate the retrieved results, Xu et al. (2015) found that stereo images provide significantly better results for buildings below 50 m, while SAR images provide significantly better results for buildings above 100 m. For buildings between 50 m and 100 m, stereo images provide slightly better results than SAR images. The site-averaged vertical velocity profiles from LES outputs also demonstrate clearly that there are three levels of building heights: below 50 m, between 50 m and 100 m, and above 100 m (Fig. 12). However, the sample size of buildings above 100 m is small, as shown in the attached boxplot of Fig. 3. This is

further confirmed by the relatively small magnitude of downward motions generated by high-rise buildings above 100 m in Fig. 12. Therefore, we define lower (higher) buildings as those with a height below (above) 50 m in this study.

Tall buildings are underestimated by the stereo images, which can be seen in Fig. 3b. If we check the details of VR inside the congested urban spaces of the assessment areas (Figs. 6 and 7), a larger difference can be found in the stereo result than in the SAR result in the simulations, particularly for areas around high-rise buildings (building heights in Figs. 6 and 7 are scaled by the horizontal color bar). This implies that a better representation of higher buildings may contribute more to the quality of pedestrian-level ventilation simulations, as high-rise

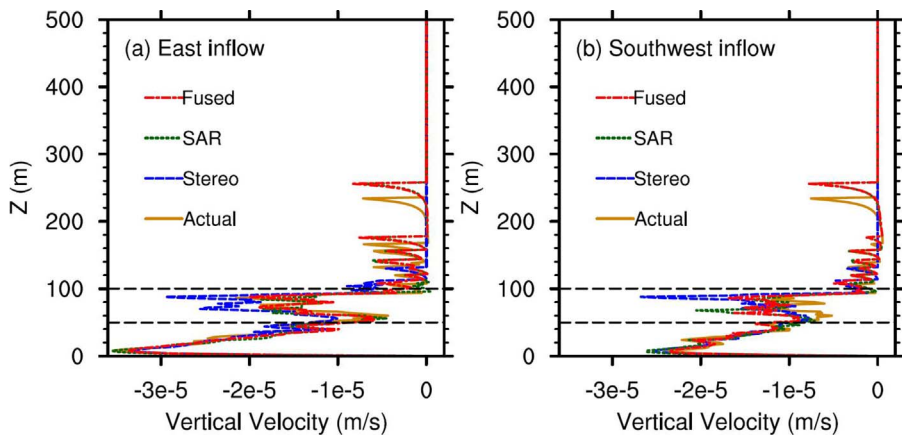


Fig. 12. Site-averaged profiles of vertical velocity (w -wind component) computed by LES in four types of building data with (a) east wind inflow, and (b) southwest wind inflow. The roughness lengths are 0.02 m. $Z = 50$ m and 100 m are indicated by horizontal black dashed lines.

buildings can experience high wind loads and concentrate pedestrian-level winds (Liu et al., 2005; Wang et al., 2017).

We further demonstrate this dynamically using an extreme case: the tallest building is at a coordinate of approximately $x = 0.55$ km, $y = 1.0$ km (Figs. 6 and 7). Fig. 13 shows the vertical velocity of the x - z cross section at $y = 1000$ m, which crosses the tallest building on the site. The results of the LES experiment with a roughness length of 0.02 m and east wind input from all four topography datasets are shown. It is obvious that both the SAR and fused results can capture the high-rise building as well as the vertical motion around it, while the stereo result fails to do so. When the wind comes from the east (right-hand side of Fig. 13), the high-rise building blocks the wind and results in strong sinking motion on its windward side and rising motion in front of its steep side and on the leeward side. This vertical motion will further induce horizontal winds and gusts at the pedestrian level and hence increase ventilation in the subdomain where the high-rise building stands. The averaged VR in the two grid boxes that are closest (on the south) to the high-rise building in Fig. 6 (the second and third grid boxes from the left in the uppermost row), for instance, is 0.21 in the actual case, while it is approximately 50% lower, 10% higher, and 14% higher in the stereo, SAR, and fused results, respectively. It is also

noteworthy that a similar structure of vertical motion can be found around other high buildings (above 50 m) in Fig. 13, which suggests that better performance in representing higher buildings, rather than lower buildings, is more important in building height extraction for AVA purposes.

4.4. Improvements in satellite image fusion

In this study, actual building footprints are given before building heights are extracted from satellite images; therefore, there is no difference in building coverage ratios in data from different sources. Other than coverage ratio, FAI is found to be another important morphological factor that influences urban ventilation (Ng et al., 2011; Razak et al., 2013). Fig. 10 evaluates FAIs computed from different satellite-retrieved data. Fig. 10 suggests that SAR images perform better than the stereo images, and the fused result shows a slight improvement over the retrieval of a single type of image (larger R^2 with both east and southwest wind). However, this slight improvement of the fused images cannot improve the pedestrian-level ventilation performance in the LES, as discussed above (Table 2, Figs. 8 and 9). But improvements are found in reproducing the horizontally averaged

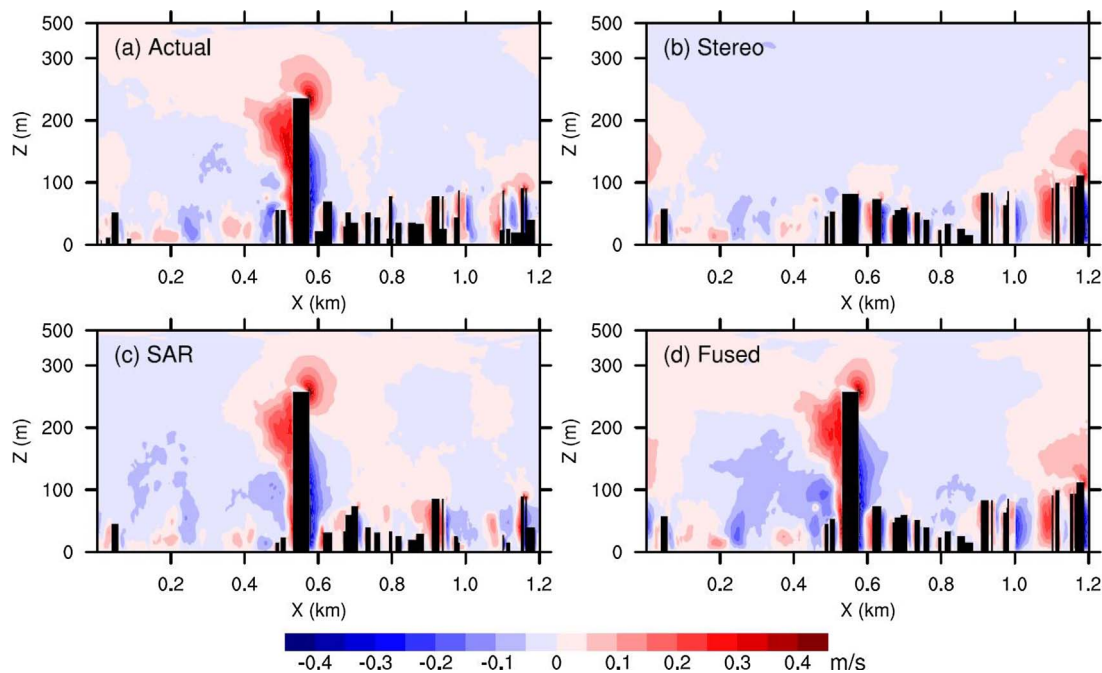


Fig. 13. Time-averaged vertical velocity in a specific section with a high-rise building from (a) actual urban elevations, and urban elevations extracted from (b) stereo images, (c) SAR images, and (d) fused results of the two images. The roughness length is 0.02 m and wind input is from the east (right).

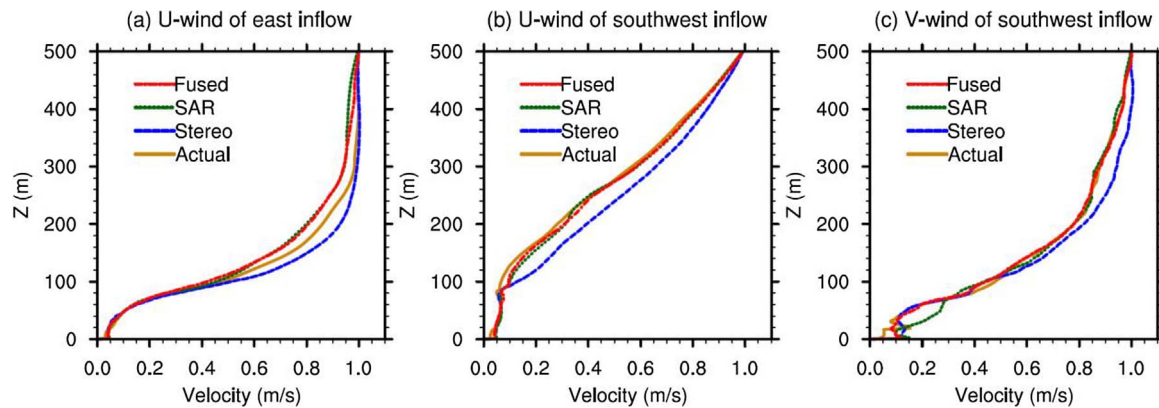


Fig. 14. Horizontally averaged wind profile within the canopy normalized by the velocity at the canopy top (500 m). (a) U-wind of wind input from the east, (b) U-wind of wind input from the southwest, and (c) V-wind of wind input from the southwest. Roughness lengths are 0.02 m.

velocity profiles (Fig. 14). Fig. 14 shows that the performance in reproducing the horizontally averaged profiles of u- and v-wind components in the canopy layer is generally consistent with the performance in capturing pedestrian-level VR. The result from stereo data has a larger discrepancy from the actual compared to the SAR and fused data. But in Fig. 14c, the dashed green line shows a large discrepancy in the lower layers, specifically, between 20 m and 60 m. At this aspect, the fusion of the two types of satellite images is superior to the retrieval from a single type. Furthermore, stereo images are required in the next step of extracting building footprints (Xu et al., 2017).

5. Discussion

Extraction of urban information from satellite images has become a hot topic in remote-sensing studies (Colin-Koeniguer & Trouve, 2014; Jin & Davis, 2005; Sportouche et al., 2011; Zhou & Zhou, 2014), as these techniques are important for urban studies (Ren, Ng, & Katzschner, 2011). Therefore, assessment of these techniques should be done in combination with urban applications, which is the origin of the present study. As a case study, building information in a high-density urban area in Mong Kok, Hong Kong, including both actual information and that retrieved from satellite images, is adopted from a newly published report (Xu et al., 2015) and is evaluated by comparing pedestrian-level ventilation in an LES model. This is challenging because urban wind environments are extremely sensitive to urban morphologies and building geometries (Shi et al., 2015; Yang, Qian, & Lau, 2013). The accuracy requirement of urban geometries and building heights for AVA studies may be higher than that for other studies, such as thermal analysis that does not consider wind effects. As one can imagine, the effects of buildings on thermal conditions arise mainly through shading and anthropogenic heat generated by the buildings, and these effects are more localized than effects of building geometries on the wind environment.

We first consider site-averaged VR and evaluate the effect of average size for the calculation. In Section 4.1, we deem that the effects of average size, 50 m × 50 m or 100 m × 100 m, on the overall RMSEs are not significant, as these two average sizes do not practically change the order of RMSEs from the three sets of topography in Table 2. Therefore, the 50 m × 50 m average size is used to plot Figs. 8 and 9. These scatter plots and linear regressions demonstrate that stereo images perform poorly, while SAR images and the fused images are sufficient for the task. Such findings contribute to the effects of building height in Section 4.3, where we suggest that better performance in representing higher buildings, rather than lower buildings, is more important in building height extraction for AVA purposes. Higher (lower) buildings are defined as those with a height above (below) 50 m in this study.

Moreover, our results show that simulated pedestrian-level wind

speed is sensitive to the given wind direction and roughness length (Section 4.2), which are sensitive to building geometries. It is noteworthy that the term “roughness length” in this study is not the city-scale roughness length that is applied in wind tunnel tests, but the so-called “local roughness length” that is imposed in each local grid box adjacent to a horizontal or vertical surface (Letzel et al., 2012). The parameter is applied to every single grid point near the surfaces, including floors, walls, and roofs, in the LES model. Some urban structures may not be included in the digital elevation data, or may be subgrid-scale in CFD simulations. The ubiquitous projecting obstructions in Hong Kong, for instance, are not included in the digital elevation data, yet they have the potential to slow down the wind. One interesting finding of this study is the significance of this local roughness length, which has generally been ignored in wind tunnel tests and previous CFD studies of urban ventilation.

The city-scale roughness length in front of the targeted area (a city or a neighbourhood) for generating the input wind profile in wind tunnel tests or CFD is not involved in the LES experiments in this study. As mentioned, a vertically unique wind velocity is imposed. Associated with the cyclic boundary condition setting and adequate time (4 h) for turbulence spin-up, a sufficient vertical wind profile can be generated in the simulation, as shown in Fig. 14. Fig. 14 further demonstrates that the performance in reproducing the horizontally averaged velocity profile in the canopy layer is generally consistent with the performance in pedestrian-level VR. The result from stereo data has a larger discrepancy from the actual compared to the SAR and fused data. One exception is found in Fig. 14c, where the dashed green line shows a large discrepancy in the layer between 20 m and 60 m. We consider this one way in which the simulated results demonstrate that the fusion of two types of satellite images is superior to the retrieval from a single type.

Finally, studies of urban wind environments using the LES technique require accurate urban morphologies and building geometries, that is, precise urban elevation data. For the retrieved data used in this study, building footprints are assumed to be known before the building heights are extracted. Hence the street patterns are basically the same among all four sets of data evaluated in this study, and differences in pedestrian VR are caused mainly by building height and building volume differences. However, building footprints are probably not known, in the case of not knowing the realistic elevation data. Building height retrievals from satellite images without knowing building footprints and corresponding evaluations from the perspective of urban applications should be initiated in further studies.

6. Conclusions

This study performs a set of LES experiments to evaluate building height extraction from satellite images in an urban area of Mong Kok,

Hong Kong. This comparative study is done from the practical perspective of urban ventilation. Major findings and recommendations can be summarized as follows: First, zonal comparison of wind tunnel tests and LES results suggests that a roughness length of 0.02 m in the LES gives more comparative results of the two (Fig. 4). Second, the choice of average size (50 m × 50 m or 100 m × 100 m) causes no significant change in the LES-computed ventilation performance of different satellite-derived building data (Table 2). Third, the effect of roughness length is rather case-dependent and highly associated with building shape and input wind direction (Fig. 11). Fourth, building heights extracted from the stereo image perform the worst compared to those from the SAR image and the fused result of both images. Both the SAR and fused results can be considered acceptable for AVA purposes in this assessment (Table 2 and Figs. 8 and 9). It is known that high-rise buildings produce strong winds concentrated at the pedestrian level, and it is documented that data extracted from stereo images produce better representations of low buildings, while data extracted from SAR images provide better results with high buildings (Fig. 13). This may be the reason why a larger bias is found in the stereo result than in the SAR result in both the east and southwest wind simulations. A further implication for this point is that retrieval methods with better representation of higher buildings can obtain better CFD results for urban ventilation. Fifth, the fused building data show a slight improvement in FAIs over the retrieval from a single type of image (Fig. 10). However, this slight improvement of the fused images over the SAR images cannot improve the pedestrian-level ventilation performance in the LES. Fusion is superior to a single type of satellite image in reproducing more accurate wind profiles in the simulations (Fig. 14).

Acknowledgments

This study was supported by the Research Grants Council of the Hong Kong Special Administrative Region (Project No. 14408214), and Institute of Environment, Energy and Sustainability, CUHK (Project ID: 1907002).

References

- Arnfield, A. J. (2003). Two decades urban research: A review of turbulence, exchanges of energy and water, and the urban heat island. *International Journal of Climatology*, 23, 1–26.
- Britter, R. E., & Hanna, S. R. (2003). Flow and dispersion in urban areas. *Annual Review of Fluid Mechanics*, 35(1), 469–496.
- Castillo, M. C., Inagaki, A., & Kanda, M. (2011). The effects of inner- and outer-layer turbulence in a convective boundary layer on the near-neutral inertial sublayer over an urban-like surface. *Boundary-Layer Meteorology*, 140(3), 453–469.
- Colin-Koeniguer, E., & Trounev, N. (2014). Performance of building height estimation using high-resolution PolInSAR images. *IEEE Transactions on Geoscience and Remote Sensing*, 52(9), 5870–5879.
- Eckert, S., & Hollands, T. (2010). Comparison of automatic DSM generation modules by processing IKONOS stereo data of an urban area. *IEEE Journal of Selected Topics in Applied Earth Observation and Remote Sensing*, 3(2), 162–167.
- Emmanuel, R., & Johansson, E. (2006). Influence of urban morphology and sea breeze on hot humid microclimate: The case of Colombo, Sri Lanka. *Climate Research*, 30, 189–200.
- Hong Kong Planning Department (2008). *Working Paper 2B: Wind tunnel benchmarking studies, batch 1. Urban climatic map and standards for wind environment – Feasibility study*. Hong Kong Planning Department [pp. 587].
- Inagaki, A., Castillo, M. C. L., Yamashita, Y., Kanda, M., & Takimoto, H. (2011). Large-eddy simulation of coherent flow structures within a cubical canopy. *Boundary-Layer Meteorology*, 142(2), 207–222.
- Jin, X., & Davis, C. H. (2005). Automated building extraction from high-resolution satellite imagery in urban areas using structural, contextual, and spectral information. *EURASIP Journal on Applied Signal Processing*, 14, 2196–2206.
- Kanda, M., Inagaki, A., Miyamoto, T., Gryschka, M., & Raasch, S. (2013). A new aerodynamic parameterization for real urban surfaces. *Boundary-Layer Meteorology*, 148(2), 357–377.
- Keck, M., Raasch, S., Letzel, M. O., & Ng, E. (2014). First results of high resolution large-eddy simulations of the atmospheric boundary layer. *Journal of Heat Island Institute International*, 9(2), 39–43.
- Letzel, M. O., Krane, M., & Raasch, S. (2008). High resolution urban large-eddy simulation studies from street canyon to neighbourhood scale. *Atmospheric Environment*, 42(38), 8770–8784.
- Letzel, M. O., Helmke, C., Ng, E., An, X., Lai, A., & Raasch, S. (2012). LES case study on pedestrian level ventilation in two neighbourhoods in Hong Kong. *Meteorologische Zeitschrift*, 21(6), 575–589.
- Lindberg, F., & Grimmond, C. S. B. (2010). Continuous sky view factor maps from high resolution urban digital elevation models. *Climate Research*, 42(3), 177–183.
- Liu, H., Jiang, Y., Liang, B., Zhu, F., Zhang, B., & Sang, J. (2005). Studies on wind environment around high buildings in urban areas. *Science in China Ser. D Earth Sciences*, 48(Suppl. 2), 102–115.
- Maronga, B., Gryschka, M., Heinze, R., Hoffmann, F., Kanani-Sühring, F., Keck, M., et al. (2015). The Parallelized Large-Eddy Simulation Model (PALM) version 4.0 for atmospheric and oceanic flows: Model formulation, recent developments, and future perspectives. *Geoscientific Model Development Discussions*, 8(2), 1539–1637.
- McGill, R., Tukey, J. W., & Larsen, W. A. (1978). Variations of boxplots. *The American Statistician*, 32(1), 12–16.
- Ng, E., & Cheng, V. (2012). Urban human thermal comfort in hot and humid Hong Kong. *Energy and Buildings*, 55, 51–65.
- Ng, E., Yuan, C., Chen, L., Ren, C., & Fung, J. C. H. (2011). Improving the wind environment in high-density cities by understanding urban morphology and surface roughness: A study in Hong Kong. *Landscape and Urban Planning*, 101(1), 59–74.
- Ng, E. (2009). Policies and technical guidelines for urban planning of high-density cities – Air ventilation assessment (AVA) of Hong Kong. *Building and Environment*, 44(7), 1478–1488.
- Park, S.-B., & Baik, J.-J. (2014). Large-eddy simulations of convective boundary layers over flat and urbanlike surfaces. *Journal of the Atmospheric Sciences*, 71(5), 1880–1892.
- Park, S.-B., Baik, J.-J., Raasch, S., & Letzel, M. O. (2012). A large-eddy simulation study of thermal effects on turbulent flow and dispersion in and above a street canyon. *Journal of Applied Meteorology and Climatology*, 51(5), 829–841.
- Raasch, S., & Schröter, M. (2001). PALM – A large-eddy simulation model performing on massively parallel computers. *Meteorologische Zeitschrift*, 10, 363–372.
- Ramponi, R., Blocken, B., de Coo, L. B., & Janssen, W. D. (2015). CFD simulation of outdoor ventilation of generic urban configurations with different urban densities and equal and unequal street widths. *Building and Environment*, 92, 152–166.
- Razak, A. A., Hagishima, A., Ikegaya, N., & Tanimoto, J. (2013). Analysis of airflow over building arrays for assessment of urban wind environment. *Building and Environment*, 59, 56–65.
- Ren, C., Ng, E., & Katschner, L. (2011). Urban climatic map studies: A review. *International Journal of Climatology*, 31(15), 2213–2233.
- Rodi, W., Ferziger, J. H., Breuer, M., & Pourquie, M. (1997). Status of large eddy simulation: Results of a workshop. *Journal of Fluids Engineering*, 119(2), 248–262.
- Schatzmann, M., & Leitl, B. (2011). Issues with validation of urban flow and dispersion CFD models. *Journal of Wind Engineering and Industrial Aerodynamics*, 99(4), 169–189.
- Shi, X., Zhu, Y., Duan, J., Shao, R., & Wang, J. (2015). Assessment of pedestrian wind environment in urban planning design. *Landscape and Urban Planning*, 140, 17–28.
- Skote, M., Sandberg, M., Westerberg, U., Claesson, L., & Johansson, A. (2005). Numerical and experimental studies of wind environment in an urban morphology. *Atmospheric Environment*, 39(33), 6147–6158.
- Sportouche, H., Tupin, F., & Denise, L. (2011). Extraction and three-dimensional reconstruction of isolated buildings in urban scenes from high-resolution optical and SAR spaceborne images. *IEEE Transactions on Geoscience and Remote Sensing*, 49(10), 3932–3946.
- Tamura, T. (2008). Towards practical use of LES in wind engineering. *Journal of Wind Engineering and Industrial Aerodynamics*, 96(10–11), 1451–1471.
- Unger, J. (2004). Intra-urban relationship between surface geometry and urban heat island: Review and new approach. *Climate Research*, 27, 253–264.
- Wang, W., Zhou, W., Ng, E. Y. Y., & Xu, Y. (2016). Urban heat islands in Hong Kong: Statistical modeling and trend detection. *Natural Hazards*, 83(2), 885–907.
- Wang, W., Ng, E., Yuan, C., & Raasch, S. (2017). Large-eddy simulations of ventilation for thermal comfort—A parametric study of generic urban configurations with perpendicular approaching winds. *Urban Climate*, 20, 202–227.
- Wong, M. S., Nichol, J., & Ng, E. (2011). A study of the wall effect caused by proliferation of high-rise buildings using GIS techniques. *Landscape and Urban Planning*, 102(4), 245–253.
- Xu, Y., Ma, P., Ng, E., & Lin, H. (2015). Fusion of WorldView-2 stereo and Multitemporal TerraSAR-X images for building height extraction in urban areas. *IEEE Geoscience and Remote Sensing Letters*, 12, 1795–1799.
- Xu, Y., Ren, C., Ma, P., Ho, J., Wang, W., Lau, K. K.-L., et al. (2017). Urban morphology detection and computation for urban climate research. *Landscape and Urban Planning*, 167, 212–224.
- Yang, F., Qian, F., & Lau, S. S. Y. (2013). Urban form and density as indicators for summertime outdoor ventilation potential: A case study on high-rise housing in Shanghai. *Building and Environment*, 70, 122–137.
- Zhou, G. Q., & Zhou, X. (2014). Seamless fusion of LiDAR and aerial imagery for building extraction. *IEEE Transactions on Geoscience and Remote Sensing*, 52(11), 7393–7407.